SECTION IV

ABSTRACTS OF PAPERS IN PRESS

To be published in "Contemporary Research in Nuclear Physics"
D.H. Feng, et al, eds. Plenum Press, New York (1981)

Workshop on Nuclear Structure, Philadelphia, 1-4 September, 1980

THE INTERACTING-BOSON-FERMION APPROXIMATION

O. Scholten

Cyclotron Laboratory
Michigan State University
East Lansing, Michigan 48824

I. INTRODUCTION

In this contribution the extension will be discussed of the Interacting Boson Approximation (IBA) model to odd-A nuclei where the fermion degrees of freedom need to be considered explicitly. The IBA model describes even-even nuclei as a system of interacting s- and d-boson. By coupling the degrees of freedom of a single nucleon to these bosons one can describe also odd-A nuclei. The general Hamiltonian for this coupled system can be written as

$$H = H_B + H_F + V_{BF} \tag{1}$$

The IBA Hamiltonian, H_B, describes the system of s- and d-bosons. H_F is the Hamiltonian for the single odd particle and thus contains only a one-body term

$$H_F = \sum_{j,m} \epsilon_j a^\dagger_{jm} a_{jm} \tag{2}$$

In our convention the summation index j denotes the shell model orbits in the valence shell. The quasi-particle energies are denoted by ϵ_j.

The most general two-body boson-fermion interaction is given in Ref.1. In this formulation the physical interpretation of the various terms is not very transparent and it is impractical to give a phenomenological description of odd-A nuclei. In the

To be published in "Contemporary Research in Nuclear Physics"
D.H. Feng, et al, eds. Plenum Press, New York (1981)

Workshop on Nuclear Structure, Philadelphia, 1-4 September, 1980

Charge Evolution of High-Energy Heavy-Ion Collisions Studied through Low-Energy $\pi^{\pm}$ Spectra

K. Frankel[a], J. Rasmussen[a], J. Sullivan[a], H. Bowman[a], D. Murphy[a], O. Hashimoto[a,b], M. Koike[b], K. Crowe[a], J. Bistirlich[a], W. Zajc[a], J. Martoff[a], R. Bossingham[a], J. Peter[c], J. Quebert[d], W. Benenson[e], G. Crawley[e], E. Kashy[e] and J. Nolen[e]

a) Lawrence Berkeley Laboratory, Berkeley, CA 94720

b) Institute for Nuclear Study, Univ. of Tokyo, Tanashi, Tokyo 188, Japan

c) Institute de Physique Nucleaire, Orsay, France

d) Centre d'Etude Nucleaires de Bordeaux Gradignan, France

e) Michigan State University, E. Lansing, MI 48824

McGraw Hill Encyclopedia of Science and Technology (1981)
David K. Scott

SPALLATION REACTION

A nuclear reaction in which the interacting nuclei are disintegrated into a large number of the constituent protons, neutrons and other light particles. Compared to more conventional reactions involving the simple transfer of nucleons between the colliding nuclei, spallation is a violent process occurring at high incident energy. An extreme case is illustrated in Fig. 1, which shows the interaction of an Argon nucleus (18 protons and 22 neutrons) with a Lead nucleus (82 protons and 126 neutrons) in a Streamer Chamber at an incident energy of 72,000 MeV. The emitted charged particles appear as tracks of electrical discharge in a gas. In this example the nuclei are apparently completely shattered into individual nucleons. Spallation can also be induced by lighter particles, such as high energy protons; however, these reactions are usually less violent and produce only a few particles (typically 3 to 10). Although the most abundant final products are protons, neutrons and alpha particles, the spallation of larger fragments like lithium and carbon also occurs. The short, thick tracks in Fig. 1 are probably created by the emission of these larger chunks of nuclear matter.

The detailed mechanism whereby the incident energy is communicated to the nuclei in the spallation process is not well understood, but there may well be analogies with the breakup of other forms of matter.

MSUCL-343
December 1980

Precompound Emission of Light Particles in the Reaction $^{16}O + ^{238}U$ at 20 MeV/u

T.C. Awes, G. Poggi[+], and C.K. Gelbke[++]

Cyclotron Laboratory, Michigan State University
East Lansing, Michigan 48824

B.B. Back and B. G. Glagola

Chemistry Division, Argonne National Laboratory
Argonne, Illinois 60439

H. Breuer and V.E. Viola, Jr.[+++]

Departments of Physics and Chemistry
University of Maryland, College Park, Maryland 20742

[+]On leave from the University of Florence, Italy

[++]Alfred P. Sloan Fellow

[+++]John Simon Guggenheim Fellow, present address:
Department of Chemistry, Indiana University,
Bloomington, Indiana 47401

ABSTRACT

Double differential cross sections have been measured for energetic p, d, t and α particles emitted in reactions of 315 MeV ^{16}O ions on ^{238}U. In coincidence with light-particle emission the momentum transfer to the target is determined by measuring the folding angle between the two fission fragments resulting from the sequential decay of the target nucleus. It is concluded that the emission of these particles occurs predominantly in fusion-type "central" collisions and at an early stage of the reaction. The energy and angular distributions are described by thermal emission from a source moving with approximately half of the beam velocity. Alternatively, the energy spectra can be explained by emission from a rotating hot spot.

The cross sections for d, t and α emission can be described in terms of a generalized form of the coalescence model which takes into account the Coulomb repulsion from the target nucleus.

MSUCL-346
February 1981

A Surface Ionization Source for Beam Energy Calibration

P. Dyer and R.G.H. Robertson

Cyclotron Laboratory and Department of Physics
Michigan State University
East Lansing, Michigan 48824, USA

Abstract

A surface ionization source has been constructed to produce Tl^+ ions having the same magnetic rigidity as light ions of a few MeV energy. The light-ion energy is determined by matching the paths of the light and Tl^+ ions through a magnetic spectrometer and by measuring the source voltage with a precision voltage divider and voltmeter. The absolute calibration has been verified by measuring the energy of alpha particles from a ^{212}Bi source and by measuring the $^{14}N(p,n)^{14}O$ reaction threshold.

1. Introduction

In the attempt to measure hadronic neutral current parity violation in the inverse alpha decay of the 3.563-MeV, 0^+ state of ^6Li, we search for a resonance in the $^2H(\alpha,\gamma)^6Li$ reaction at E_α = 6.238 MeV (lab energy).[1] It is required that the beam energy be known with an absolute accuracy of about 2 parts in 10^4 and that it be possible to match the beam energy from one data acquisition period to the next with an accuracy of 1 part in 10^4. In order to eliminate the uncertainties in the calibration of the accelerator beam analyzing magnet, especially those involved in interpolating or extrapolating calibration measurements at other energies, we have designed a system with which we can frequently (and with little effort) measure the energy of the beam at the $^2H(\alpha,\gamma)^6Li$ resonance energy.

For this purpose we built a surface ionization source. The source, operating at 30.47 kV, produced Tl^+ ions of the same magnetic rigidity as the 6.238-MeV α^{++} beam. Both beams could be brought down the beam line and through a Q3D spectrometer[2] to the focal plane, where the beam energy was measured by matching currents on the two halves of a split Faraday cup and measuring the voltage applied to the source extraction electrode with an accuracy of 0.01%.

The source is described in Section II, the procedure for its use is given in Section III, and two measurements for checking the absolute accuracy are given in Section IV (^{212}Bi source alpha particle energy measurements) and Section V

MSUCL-348
March 1981

Limit on Charge Symmetry Breaking in the Optical Model and the Coulomb Energy Anomaly

R.P. DeVito[a], Sam M. Austin, W. Sterrenburg[b] and U.E.P. Berg[c]
Cyclotron Laboratory and Physics Department,
Michigan State University
East Lansing, Michigan 48824

ABSTRACT

Cross sections for elastic scattering of neutrons from ^{40}Ca have been measured at 30.3 and 40.0 MeV and analyzed to obtain optical model potentials. The optical potentials for neutron and proton scattering are found to be very similar after a correction for Coulomb effects, indicating that a static charge symmetry breaking Hartree potential is too small to explain the Coulomb energy anomaly for bound states.

PACS Categories: 21.30+y; 24.40.Dn; 24.10.Ht; 21.10.Dr; 25.40Cm

At first glance it seems that it should be simple to calculate the difference in the masses of two mirror nuclei such as ^{3}H and ^{3}He or ^{41}Ca and ^{41}Sc. That simple approaches fail, by more than 500 keV in the case of the ^{41}Ca-^{41}Sc pair, was first pointed out by Nolen and Schiffer[1] and this difference became known as the Coulomb-energy or Nolen-Schiffer anomaly. In spite of an intense theoretical effort since this discovery[2], and the calculation of many small (and mostly cancelling) corrections, the problem remains. In a survey of the situation, Negele[3] concluded that the only apparent solution was to introduce a small charge symmetry breaking (CSB) potential in the nucleon-nucleon interaction, such that the strong interaction between two neutrons (V^{nn}) is more attractive than that between two protons (V^{pp}). As a result, the extra neutron in ^{41}Ca is bound more tightly than the proton in ^{41}Sc, reducing the discrepancy. In a schematic Hartree model, Negele showed that a difference of about 20 MeV-fm^3 in the volume integrals of V^{pp} and V^{nn} is sufficient to remove the anomaly. A difference of this size is not predicted by the usual theoretical models[2,4] but is consistent with experimental determinations of the scattering lengths and effective ranges for the nn and pp systems[4].

Of course, a charge symmetry breaking potential such as that proposed by Negele[3] will affect not only the

Physics Letters B

June 1981
MSUCL-351

Trends of light particle spectra observed in nucleus-nucleus collisions

T.C. Awes, G. Poggi,[+] S. Saini[++] and C.K. Gelbke[+++]

Cyclotron Laboratory, Michigan State University
East Lansing, Michigan 48824 USA

and

R. Legrain[‡] and G.D. Westfall

Lawrence Berkeley Laboratory, Berkeley, California 94720 USA

+ On leave from University of Florence, Italy

++ On leave from Bhabha Atomic Research Center, India

+++ Alfred P. Sloan Fellow

‡ On leave from C.E.N. Saclay, France

Abstract

The emission of energetic light particles (p,d,t) has been studied for ^{16}O induced reactions on Al, Zr and Au targets at the incident energies of 140, 215 and 310 MeV. The light particle energy spectra have been analyzed in terms of a moving thermal source. The apparent temperatures exhibit a systematic variation as a function of the incident energy per nucleon above the Coulomb barrier. The observed trend can be extrapolated in a smooth fashion to temperatures obtained in relativistic heavy ion collisions.

Information about the early stages of heavy-ion induced reactions may be obtained from the detection of energetic light particles which cannot be associated with evaporation from the compound nucleus.[1-5] At low energies (E/A≤20 MeV), recent experiments[4-10] have mainly used coincidence techniques to study detailed aspects of the reaction mechanisms producing energetic light particles. However, few single particle inclusive measurements have been published in this energy domain[1,11,12] and little information is available about the dependence of non-compound light particle emission on projectile, target and beam energy. In this communication, we report some of the results obtained from a survey of ^{16}O induced reactions on Al, Zr, and Au targets at 140, 215, and 310 MeV beam energy.

MSUCL-353
July 1981

Higher Order Deformations of ^{232}Th and ^{234,236,238}U

R.M. Ronningen, R.C. Melin,[a] J.A. Nolen, Jr.,
and G.M. Crawley

Physics Department and Cyclotron Laboratory
Michigan State University
East Lansing, MI 48824

and

C.E. Bemis, Jr.
Physics Division
Oak Ridge National Laboratory[b]
Oak Ridge, Tennessee 37830

We have measured the inelastic scattering of 35 MeV protons from ^{232}Th and ^{234,236,238}U. Angular distributions were extracted for $J^\pi = 0^+ - 8^+$ members of the ground state rotational bands, and were analyzed using coupled channels calculations for scattering from a deformed optical potential. The deformation parameter β_6 is positive for ^{232}Th and ^{234}U, nearly zero for ^{236}U, and negative for ^{238}U. The trends of the deformation parameters and multipole moments are explained qualitatively by a simple model.

PACS Numbers: 2.540.Ep, 27.90.+b, 21.10.Ft

The actinide nuclei accessible to scattering experiments are known to be intrinsically deformed and thus their charge and matter (proton and neutron) distributions possess nonzero multipole moments. The moments best studied experimentally and theoretically are the quadrupole and hexadecapole ("2^λ-pole", where λ=2 and 4, respectively). Very little information currently exists on higher order deformations such as the λ=6 (hexacontatetrapole).[1] The present work[2] establishes the systematic variation of the λ=6 deformation for the nuclei ^{232}Th, and ^{234,236,238}U.

Apart from the fundamental interest in the nuclear shape the importance of studying deformations of higher order than quadrupole is reflected in the effects they have on nuclear properties. For example, in the heavy transition metals (e.g. W,Os) a stability against oblate ground state shapes may be attributed to the hexadecapole degree of freedom.[3] Indeed, experimental knowledge of higher order equilibrium deformations of the actinides can put stringent constraints on theoretical methods for calculating ground state properties (and thus influences predictions concerning the stability of heavy nuclei). For example, two approaches[4] to the liquid drop contribution to ground state energies which give almost the same quadrupole deformations yield substantially different higher-order equilibrium deformations. Furthermore, rotational bands built upon single particle states[5] and the sizes of gaps in single particle energies at Z=100 and N=152 depend[3] upon the amount of λ=6 deformation.

MSUCL-347
MSUNC-220

THE ϵ/β^+ DECAY OF ^{145}Gd: RESOLUTION OF ϵ/β^+ DECAY BRANCHING RATIO ANOMALIES AND EVIDENCE FOR PRONOUNCED STRUCTURES IN THE β-DECAY STRENGTH

R.B. Firestone,[a] R.C. Pardo,[b] R.A. Warner,[c] Wm. C. McHarris, and W.H. Kelly[d]

National Superconducting Cyclotron Laboratory and
Departments of Chemistry and Physics
Michigan State University
East Lansing, Michigan 48824

[a]Present Address: Nuclear Science Division, Lawrence Berkeley Laboratory, University of California, Berkeley, CA 94720.

[b]Present Address: Physics Division, Argonne National Laboratory, Argonne, IL 60439.

[c]Present Address: Battelle Northwest, 320 Bldg.-300 Area, P.O. Box 999, Richland, WA 99352.

[d]Present Address: Department of Physics and Office of the Dean, College of Letters and Science, Montana State University, Bozeman, MT 59717.

ABSTRACT

The ϵ/β^+ decay of 23.0 min ^{145}Gd has been thoroughly studied with Ge(Li) and plastic scintillator detectors. A total of 326 γ rays de-exciting 136 levels in ^{145}Eu have been placed by this work. The available decay energy, Q_ϵ=5.07±0.06 MeV, was measured by β-γ coincidence techniques. ϵ/β^+-decay branching ratios have been measured for several transitions, and a long standing anomaly in those ratios has been resolved by the new Q_ϵ value and the discovery of additional electron-capture decay. We have investigated the β-strength function for ^{145}Gd and discovered pronounced structure with resonances at 1042, 1819, 2484, and 4500 keV. The 1042-keV resonance is proposed to result from a $(\pi d_{3/2})^2(\nu s_{1/2})^{-1}\rightarrow(\pi d_{3/2})^1$ β-transition, the 1919- and 2584-keV resonances from $(\pi d_{5/2})^2\rightarrow[(\pi d_{5/2})\otimes 2^+]_1$, decays, and the very strong 4500-keV resonance from the $(\pi h_{11/2})^2\rightarrow(\pi h_{11/2})\otimes(\nu h_{9/2}+\nu f_{7/2}+\ldots)$ transition across the shell closure.

[RADIOACTIVITY ^{145}Gd; measured E_γ, γ-γ coin, E_β, β-γ coin, Q, $t_{1/2}$, x-γ coin, $\gamma^\pm$-γ coin; deduced ϵ/β^+ ratios, logft, β-strength function, missing continuum decay intensity. ^{145}Eu; deduced levels, J, π; calculated level energies with shell model, weak-coupling model.]

J. M. Tiedje. 1981. Use of nitrogen-13 and nitrogen-15 in studies on the dissimilatory fate of nitrate. In Genetic engineering of symbiotic nitrogen fixation and conservation fo fixed nitrogen. Plenum Publ., New York.

USE OF NITROGEN-13 and NITROGEN-15 IN STUDIES ON THE DISSIMILATORY FATE OF NITRATE

James M. Tiedje

Departments of Crop and Soil Sciences and of
Microbiology and Public Health
Michigan State University
East Lansing, Michigan 48824

INTRODUCTION

Nitrate is a central nitrogen species in the biogeochemical nitrogen cycle because it is mobile, a biological oxidant, and a nitrogen source for growth for many organisms. As a result it has many competing fates. The five principle fates of soil nitrate are illustrated in Figure 1.

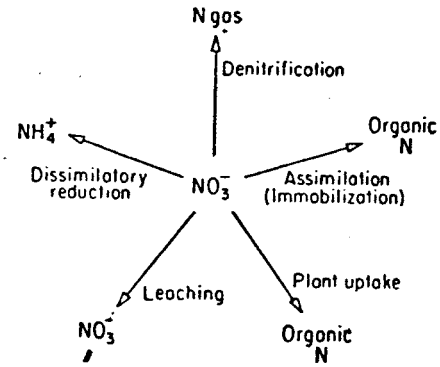

Fig. 1. Competing fates of nitrate in soil.

The top three processes are microbial and occur in soil. The subsequent fate of the metabolized N depends upon the chemical properties of the product: nitrogen gas diffuses out of the soil, ammonium is retained on clays via cation exchange, and organic-N becomes immobilized as part of soil organic matter through portions of it are slowly mineralized. The bottom two fates transport N out of the soil: plant uptake moves nitrogen to the surface where it is grazed or harvested though a portion is returned to the soil as organic nitrogen, and leaching carries nitrate below the rooting zone where it is often lost to groundwater.

In agriculture people attempt to manage these competing fates for a more favorable economic product while in natural ecosystems a quasi steady state has evolved in which stability is the optimized product. People use the imput of energy to alter the natural steady state. Agricultural practices of the past--plant variety development, cultivation, water management, weed control, fertilization--all affect this competition. The goals of the future are basically no different: they are to continue to alter the fate of nitrogen so that humans' products are favored. Obviously, one wants to increase plant recovery of nitrogen at the expense of the permanent losses, especially denitrification.

In Recent Developments in Biological and Chemical Research with Short-Lived Isotopes. K. A. Krohn and J. W. Root (ed.) Advances in Chemistry, Amer. Chem. Soc., Washington. (1981)

Use of Nitrogen-13 in Studies of Denitrification

J. M. Tiedje, R. B. Firestone, M. K. Firestone,
M. R. Betlach, H. F. Kaspar, and J. Sørensen.

Departments of Crop and Soil Sciences,
Microbiology and Public Health, and Cyclotron Laboratory
Michigan State University
East Lansing, Michigan 48824

Current locations of coauthors: R. B. Firestone, Lawrence Berkeley Laboratory, Berkeley, CA; M. K. Firestone, University of California, Berkeley, CA; M. R. Betlach, NASA Ames Research Center, Moffett Field, CA; H. F. Kaspar, Cawthron Inst., Nelson, New Zealand; J. Sørensen, University of Aarhus, Aarhus, Denmark.

QUENCHING OF MAGNETIC TRANSITIONS AND Δ(1232) DEGREES OF FREEDOM IN NUCLEI: THE ^{48}Ca CASE [+)]

A. Härting and W. Weise
Institute of Theoretical Physics
University of Regensburg, D - 8400 Regensburg, W. Germany

H. Toki
Cyclotron Laboratory, Michigan State University,
East Lansing, Michigan 48 824, USA

A. Richter
Institut für Kernphysik,
Technische Hochschule Darmstadt, W. Germany

Abstract: The quenching of M1 transitions is discussed within the framework of an effective magnetic transition operator renormalized by virtual Δ(1232)-hole excitations. This scheme is applied to the M1 transition from the ground state to the 10.23MeV (1^+) state in ^{48}Ca, a case which appears to reveal a comparatively simple shell model structure. It is demonstrated that a large fraction of the observed quenching of the B(M1) value can be related to Δ(1232) degrees of freedom in a way consistent with the quenching of Gamow-Teller transitions.

+) Work supported in part by Deutsche Forschungsgemeinschaft.

PROXIMITY TO THE RHO MESON CONDENSATION THRESHOLD IN NUCLEI

H. Toki

National Superconducting Cyclotron Laboratory
and Department of Physics
Michigan State University
East Lansing, Michigan 48824

and

J.R. Comfort

Department of Physics and Astronomy
University of Pittsburgh
Pittsburgh, Pennsylvania 15260

Abstract

Critical conditions for instability in the isovector unnatural-parity channel in nuclei are investigated in terms of the RPA. The particle-hole residual interaction consists of the π and $\rho(2\pi)$ meson-exchange attractive components in addition to the short-range repulsive Landau term. It is found that the non-resonant part of the iterated two-pion exchange moves the characteristics of the nuclear phase transition closer to those for rho-meson condensation. This mode may dominate at high density.

PACS numbers: 21.30.+y, 21.65.+f

PIONIC MODES OF EXCITATION IN NUCLEI [+)]

E. Oset [++)]
Department of Atomic and Nuclear Physics,
University of Salamanca, Spain

H. Toki
Cyclotron Laboratory, Dept. of Physics,
Michigan State University,
East Lansing, Michigan 48824, USA

W. Weise
Institute of Theoretical Physics
University of Regensburg
D - 8400 Regensburg, West Germany

(Prepared for Physics Reports)

+) Work supported in part by German Bundesministerium für Forschung und Technologie (grant no. MEP 3200 X) and by Deutsche Forschungsgemeinschaft (grant no. We 655/7-4)

++) Supported in part by Fundacion March

List of contents

1. Introduction

2. Basic Meson-Baryon Effective Lagrangians and Elementary Processes
   - 2.1 Pion-nucleon scattering
     - 2.1.1 The s-wave πN-interaction
     - 2.1.2 p-wave πN-scattering
   - 2.2 Pion-Baryon vertex factors
   - 2.3 The spin-isospin dependent Baryon-Baryon interaction
   - 2.4 The NN ↔ dπ reaction
   - 2.5 Chiral symmetry and quark model aspects of the πN interaction
     - 2.5.1 Chiral symmetry
     - 2.5.2 Outlook on quark model aspects

3. Pions in Nuclear Matter
   - 3.1 The spectrum of pion-like excitations in nuclear matter
   - 3.2 Nuclear Spin-Isospin correlations
   - 3.3 Summary

4. Pion-nuclear elastic scattering
   - 4.1 Optical potential phenomenology for pionic atoms and low energy pion-nucleus scattering
   - 4.2 Interpretation of optical potential parameters at low energy
   - 4.3 Scattering in the 3.3 resonance region
   - 4.4 Isobar-doorway phenomenology and microscopic approaches: a brief survey

5. Many-body approach to pion-nucleus scattering
   - 5.1 Δ-hole excitations and the optical potential
   - 5.2 Coherent multiple scattering in the Δ-hole model
   - 5.3 Δ-hole interactions and the Lorentz-Lorenz correction
   - 5.4 True absorption and other many-body corrections
     - 5.4.1 Pauli blocking and binding corrections
     - 5.4.2 Absorptive damping and other mechanisms
     - 5.4.3 Many-body corrections and the Δ spreading potential
   - 5.5 The complete Δ-hole model

FINAL DESIGN OF THE MAGNETIC FIELD FOR THE K-800 SUPERCONDUCTING CYCLOTRON AT MSU

F.G. Resmini, G. Bellomo, H.G. Blosser, E. Fabrici, D. Johnson

Cyclotron Laboratory, Michigan State University
East Lansing, MI 48824

Introduction

Substantial progress has been made in recent months in the design of the K800 cyclotron at MSU. As a consequence, the geometry is somewhat different from that outlined in (1) with implications on magnetic field properties, beam dynamics and extraction. Injection of beams from the K500 has not been affected by said modifications and we refer to (2) for all details.

It is the purpose of this paper to review the finalized design of the K800 and the rationale for the choices which have been made, together with their implications on the machine performance.

Review of the K800 Characteristics

As well known, the K800 is mainly intended as a booster for the K500 cyclotron, now near completion, although operation with an internal ion source is also anticipated. The energies will be 200 MeV/n for fully stripped light ions and up to 30 MeV/n for heavy ions, depending upon the available charge states from the K500.

The parameters of the machine are listed in Table I. The main differences with respect to ref. 1 are:

- the increase in pole radius from 41" to 42",
- the increase in the hill gap from 2.5" to 3",
- the increase in the hill width, at outer radii, from 46° to 51°.

The rationale for these choices will be discussed later. The operating diagram in the (B_o, Z/A) plane is shown in Fig. 1, all limits are indicated in a straightforward way.

Table I. Main K800 Parameters.

Pole radius	: 42"
Sectors	: 3, 46° wide, up to R=37.15". Flaring to 51° wide between R=37.15" and R=40.2".
Spiral constant	: 1/13 rad/inch (approx)
Minimum hill gap	: 3"
Maximum valley gap	: 36"
Min-max operating average field	: 30-50 kgauss
Yoke height	: 115"
Yoke inner and outer diameters	: 118" - 175"
R.F. frequency range	: 9-32 MHz
Harmonic operating modes	: 1st, 2nd
Peak dee voltage	: 200 kV
No of trim coils	: 22
Max current in any trim coil	: 400A
Max total trim coil power	: 70 kW
K at 50 kgauss	: 1200
$K_{Focusing}$	: 400

Twelve ions were chosen as representative ones on the operating diagram contours, as shown by dots in Fig. 1, in order to investigate the field trimming, equilibrium orbit properties and extraction.

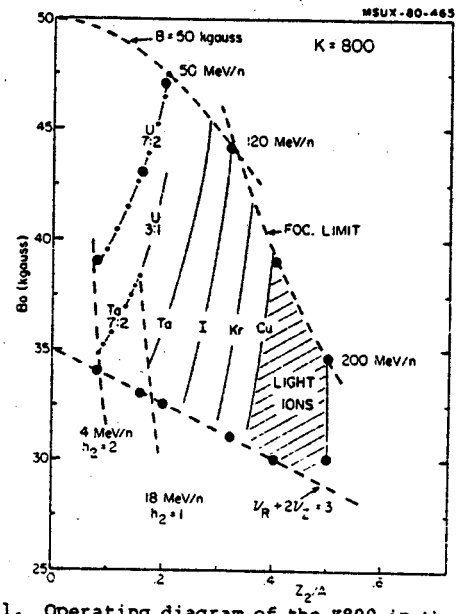

FIG. 1. Operating diagram of the K800 in the (B_o, Z/A) plane. Shown are focusing and bending limits and the low field limit due to the $\nu_R + 2\nu_V = 3$ resonance.

Main Coil Design

The coil parameters are listed in Table II. The main variation with respect to (1) is the increase of the minimum coil distance from the median plane, from 1.5" to 2". This increase allows more axial space for the insertion of the extraction elements, especially the magnetic channels, and has thus been selected. Independent excitation of the two coil sections allows proper fitting of the isochronous field for all different ions and center field values. The resulting operating

Table II. Main Coil Parameters

Inner coil radius	: 45.5"
Outer coil radius	: 51.5"
Coil total height	: 26.5"
Coil splitting	: Two sections, indep. excited
Height of section α (closer to med. plane)	: 16" (60% of total)
Height of section β (away from med. plane)	: 10.5" (40% of the total)
Minimum coil distance from med. plane	: 2"
Bobbin thickness	: .95"
Banding thickness	: 2", Aluminum alloy
Vacuum tank inner radius	: 42.25", 1" thick
Vacuum tank outer radius	: 58.5"
Cryostat total height	: 69"
Maximum current density in the coils	: 3500 A/cm^2
Amper turns at 3500 A/cm^2	: 7.2 10^6
Conductor	: NbTi, monolithic type
Conductor cross section	: .207" x .15"
Nominal Max current in conductor	: 1000 A
Overall copper to superconductor ratio	: 25:1

OPERATING EXPERIENCE WITH THE CRYOGENIC SYSTEMS FOR A SUPERCONDUCTING CYCLOTRON*

M.L. Mallory, H. Laumer, D. Poe, P. Brindza
Cyclotron Laboratory, Michigan State University
East Lansing, MI 48824

Summary

The successful operation of the superconducting cyclotron[1] cryogenic system has been primarily dependent on understanding and improving its performance. In particular, operating experience with a superconducting magnet coil, a vacuum cryopanel, and a cryogenic distribution system has been gained during the past three years. The coil cryostat cooldown, boiloff rate, warmup, eddy current pulse, median plane heat leak, and helium leakage into the cryostat vacuum jacket have been measured. The vacuum cryopanel cooldown rate, heat load, pumping speed and long term gas storage have been determined. The present measurements have been conducted with simple independent transfer lines. A subcooled cryogenic distribution system, with parallel branches, has been designed and is presently under construction.

Introduction

The general characteristics and initial operating experience of the cryogenic system for the Michigan State University superconducting magnet has been described in a previous paper.[2] This paper describes the most recent operating experience with the magnet cryostat and the results of a prototype cryopanel for the cyclotron vacuum system. In the completed cyclotron, a liquid helium distribution system must be built to deliver liquid helium to the various systems and its design is presented in the last section. The large use of cryogenics is a major part of this recent technological development in cyclotrons.

Magnet Cryostat

Over three years operating experience of the magnet cryostat has now been acquired. Various performance parameters have been measured before the cryostat was disassembled to build the extraction system penetration channels through the median plane of the liquid helium cooled coils, as well as after the cryostat reassembly. The cryostat is now in its final configuration and no more changes which affect its cryogenic performance are expected. Figure 1 is a schematic drawing of the cryostat and the instrumentation used in measuring its performance; namely, platinum thermometers, liquid helium level gauges, vacuum jacket ionization gauge and a helium mass spectrometer.

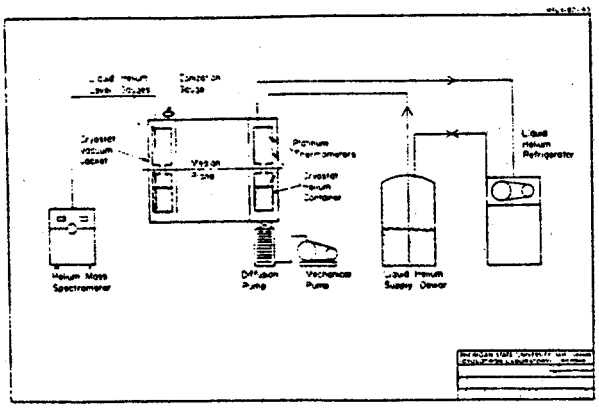

FIG. 1. A schematic drawing of the superconducting cyclotron showing the various monitoring devices used in making cryogenic measurements.

Cooldown-Warmup

Figure 2 shows the cooldown and warmup curves of temperature vs. time for the cryostat. The cooldown takes 120 hrs, and its rate is determined by the mass flow limitation of the refrigerator coldbox. The warmup of the cryostat is done by using the refrigerator to flow warm gas (~100K warmer than the coil) through the coil and returning it directly to the compressor pump suction, thereby bypassing the mass flow limitation of the refrigerator. The coil is warmed to room temperature in ~ 50 hrs.

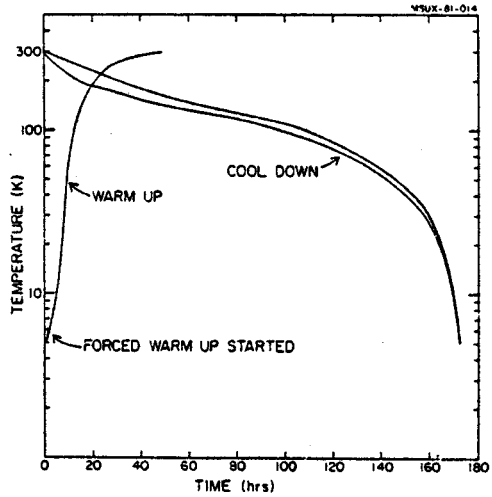

FIG. 2. The cooldown and warmup curves of the ~8 ton cryostat is shown. The cooldown is limited by the mass flow of the refrigerator.

Heat-Load

The heat load sources of the cryosystem are the transfer lines, storage system and the cryostat. The total load is less than 72 watts and more than 57 watts, determined by running the CTI 1400 refrigerator with two helium compressors and with and without liquid nitrogen.[3] The cryostat contribution to the heat load has been measured by monitoring its boiloff rate (Figure 3). It is 22 watts when the cryostat is filled to its operating level. An additional heat load due to the current leads when the magnet is at full current, is estimated to be 2 watts. In addition there is a transient heat load due to eddy current heating in the coil banding. Figure 4 shows how charging the magnet raises the helium level in the cryostat. It is proposed that the heating makes helium bubbles which then raise the helium level. A calculation of the expected thermal energy due to eddy currents is consistent with the amount of helium boiled, as estimated from the level increase. Details of the magnetic field change are consistent with the different rates of heating seen in charging and discharging the magnet.

Helium Leak

A helium leak from the coil cryostat to its vacuum jacket was detected. Figure 5 is a measurement of the pressure in the cryostat vacuum jacket; with a diffusion pump on, a pressure of $4.6 * 10^{-6}$ Torr had been attained; then the pump was closed off. A pressure increase with time indicating a helium leak rate of 10^{-10} g/s was observed. Experimental data were acquired

BEAM TRANSPORT CALCULATION FOR K-500 CYCLOTRON OPERATION AT MICHIGAN STATE UNIVERSITY

J. Kasagi, S. Angius and E. Kashy
Cyclotron Laboratory, Michigan State University
East Lansing, MI 48824

Summary

The design of the beam transport and analysis system for the experimental facility using the K-500 superconducting cyclotron at M.S.U. and which is currently being assembled is described.

Introduction

The beam transport calculation for the experimental facility using the K-500 superconducting cyclotron has been carried out by using various beams expected from the K-500 cyclotron. The final design of the beam transport and analysis system has been made from these calculations. The system not only can deliver any kind of beams from the K-500 cyclotron to the experimental area but also can provide for a variable linear dispersion at the target positions of the magnetic spectrographs. This paper describes the beam transport system which is currently being assembled.

Experimental Floor Plan for K-500 Cyclotron

The layout of the experimental floor with beam transport element is shown in Fig. 1. The experimental area is separated into two large rooms designated North and South. The South vault houses a 60 inch scattering chamber, a prototype version of the reaction product mass separator (RPMS) planned for research with the coupled superconducting cyclotrons, a gamma ray goniometer and target chamber for the cryogenic helium-jet apparatus. The North vault houses the Enge split pole spectrograph, the S320 spectrograph with a K=320 bending capacity, a scattering chamber planned for neutron experiment and a low rigidity (K=250) beam line. The S320 spectrograph is also used as a portion of the beam transport elements for the Enge split pole beam line and for the neutron chamber beam line as shown in Fig. 1.

The first section of the transport is the region from the exit of the K-500 cyclotron to the first slit position (S1). There are 6 quadrupole magnets and one small dipole magnet in this section. The beam is bent by the dipole magnet located after the S1 and distributed to each target positions by the next dipole magnet.

Beam Transport from the Cyclotorn to the Initial Waist

The properties of the beams from the K500 cyclotron were calculated by ray-tracing method.[1] In this calculation, the effect of the magnetic channels of the extraction system were included using the result of the magnetic field measurement. Eight different beams which correspond to the extreme conditions of the cyclotron were provided for the transport calculation. Table 1 shows the calculated beam properties at cyclotron exit for several beams. They are very different from each other. An unusual feature of the extraction system of the K500 cyclotron, which consists entirely of inert focusing elements, strongly influences the beam properties. This feature greatly simplifies design and construction of the extraction system itself but at the cost of a variability in direction and focusing conditions for beams leaving the cyclotron. The first section of the transport system must then be used as an active element to compensate for this variability in order to bring all beams to an approximately identical phase space condition at the location of S1.

The arrangement of the transport elements was carried out by using the code TRANSPORT.[2] The six quadrupole magnets located in this section are found to be a sufficient number of optical elements to control any beam from K-500 cyclotron to the S1 position. The resulting properties of beam 1, 5, 6 and 7 at the S1 are almost same as shown in Table 2. Figure 2 shows an example of the beam envelope of two extreme beams tracked through this section of the optical system.

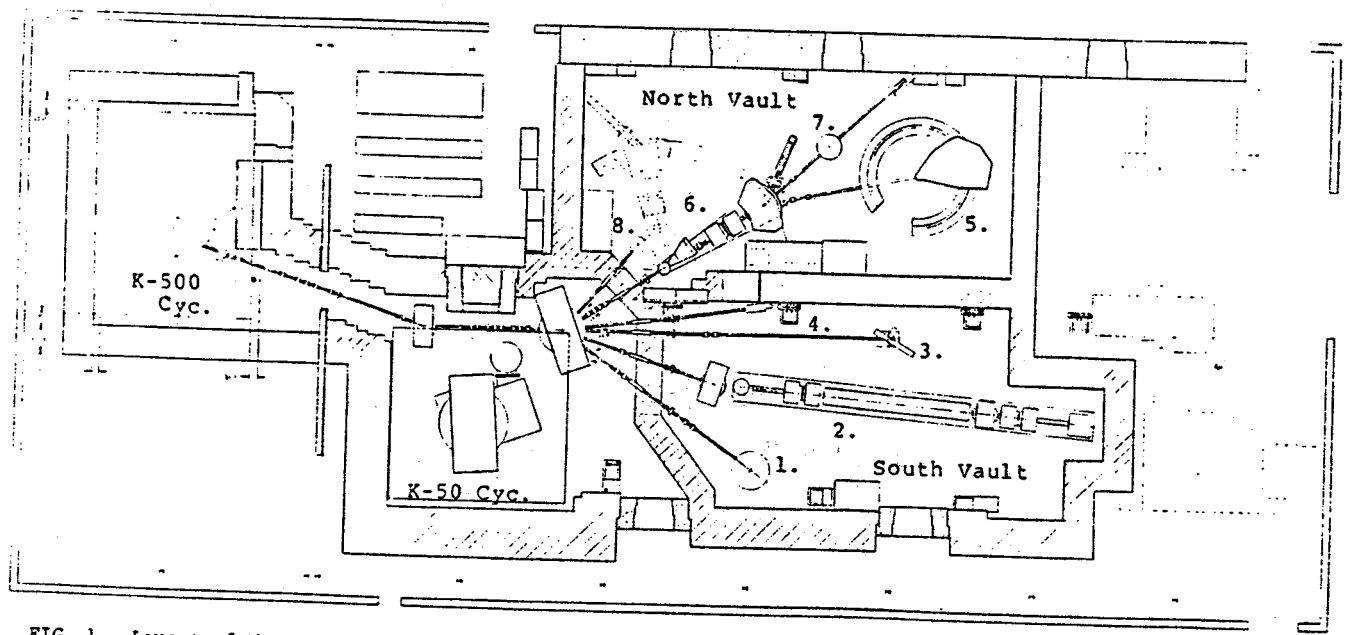

FIG. 1. Layout of the experimental floor. 1. 60 inch Scattering Chamber. 2. Recoil Product Mass Separator. 3. γ-ray Goniometer. 4. Cryogenic He Jet. 5. Enge Split-pole Spectrograph. 6. S320 Spectrograph. 7. Neutron Scattering Chamber. 8. K=250 beam line.

K-500 SUPERCONDUCTING CYCLOTRON DEFLECTOR HIGH VOLTAGE TESTS

T. Antaya, P. Miller and D. Poe
Cyclotron Laboratory, Michigan State University
East Lansing, Michigan 48824

Summary

We report measurements of electrical properties of a compact electrostatic deflector and high voltage transmission line for the K-500 cyclotron. The voltage limits, sparking rates, dark current levels and the effects of conditioning are observed. The system supports the maximum required voltage and fits within the space available at the mid-plane of the superconducting magnet. Both stainless steel and titanium are suitable anode materials. A surge-limiting resistance between power supply and deflector greatly reduces spark damage to the anode surface.

Introduction

The extraction system of the K-500 superconducting cyclotron consists of two electrostatic deflectors, eight inert iron focusing bars, and two harmonic compensation bars. The final design features are the result of extensive calculations of the extraction beam dynamics.[1] The deflectors must support voltages as high as 94 kV. The connection to the power supply penetrates the cryostat at the median plane. We must therefore compromise between thermal insulation and electrical insulation when allocating space. These requirements lead to the present coaxial design of the transmission line ("feed thru") whose essential features are indicated in Fig. 1.

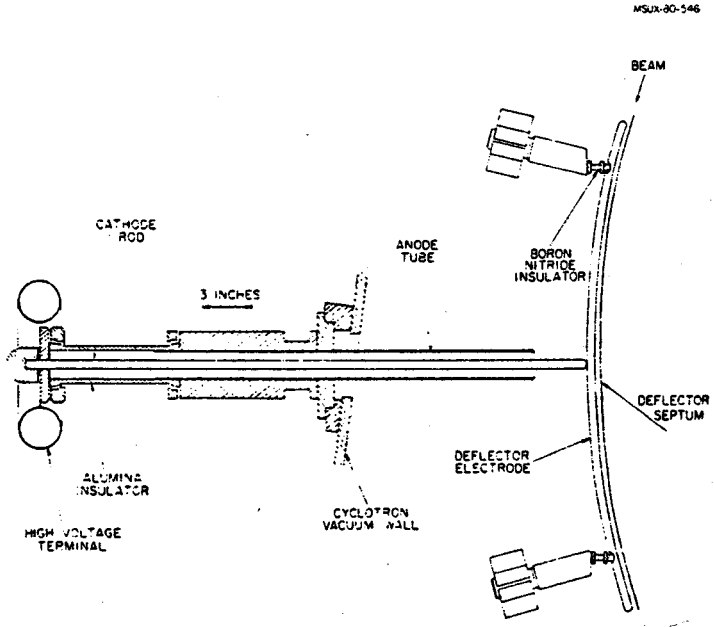

FIG. 1. The K-500 type high voltage feedthru supplies the existing 50 MeV cyclotron electrostatic deflector for feedthru high voltage testing. The center conductor length is 32 inches and will increase to 44 inches in the K-500 cyclotron. The deflector electrode is 29 inches long.

The feedthru is shown attached to the 50 MeV cyclotron deflector for tests. The center conductor and the attached deflector electrode are supported by the terminal nut at one end and the deflector insulators at the other. The anode is actually two concentric tubes, the inner a removeable spark liner.

The mechanical design of the K-500 deflector is inpart fixed by the requirement that it be moveable. The deflector electrode and septum reside in a self-contained housing. The cross-section at a mock-up deflector, as assembled for tests in the 50 MeV cyclotron, is seen in Fig. 2. The electrode cross-section and clearances are identical to those planned for the K-500 cyclotron.

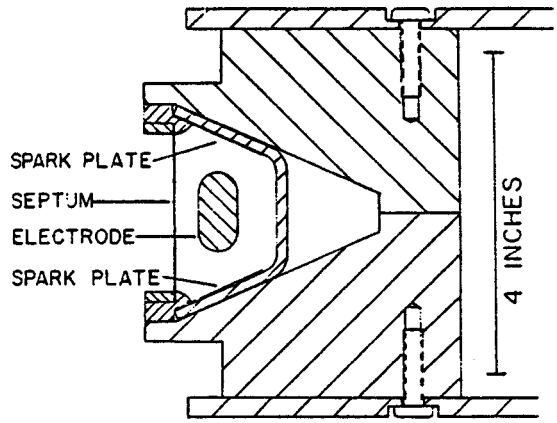

MSUX-81-058

FIG. 2. Cross-section of the K-500 style electrostatic deflector model showing the electrode geometry. The deflector electrode and septum are 7 mm apart.

Apart from the smaller axial gaps, the K-500 deflector design is a straight-forward extension of the deflector that operated for many years in the 50 MeV cyclotron (same insulators, radial gap and electrode shape). Note that water-cooling of the deflector is not provided (to save space) and it is unnecessary according to this experience. The high voltage transmission line is improved by eliminating plastic and shielding the insulator from sparks. It must also be smaller in diameter to fit through the midplane of the coil, so the electric field becomes larger than in the deflector gap. At 94 kV, the maximum electric field in the deflector is 134 kV/cm, but in the feedthru it is 172.9 kV/cm, 22% higher. The 1.25 inch outside diameter of the anode liner represents the largest tube that leaves adequate clearance. After some experimentation with larger diameter anode tubes, the objectives were accomplished for two different anode materials in the required size: (1) 304 stainless steel and (2) titanium. In both cases, the cathode material was stainless steel.

Description of the High Voltage Experiments

The experiments described here were performed in the 50 MeV cyclotron without beam present. Air pressure in the vacuum chamber was maintained at 2×10^{-5} torr by a single oil diffusion pump. Since a magnetic field influences the behavior of the deflector during sparking, we did testing with and without the magnet on. The position of the deflector relative to the average magnetic field profile is shown in Fig. 3.

Prototype Deflector Tests

The 50 MeV cyclotron deflector was replaced by a mock-up K-500 deflector assembly. The external deflector terminal, power supply connections and controls were

OPTICAL MODEL SOLUTIONS FOR PIONIC MODES IN NUCLEAR MATTER

P. Hecking
National Superconducting Cyclotron Laboratory
Michigan State University
East Lansing, Michigan 48824

Abstract

Solutions for damped plane pion waves in homogeneous nuclear matter are deduced from optical potential parameters, taken from pion scattering and pionic atom data.

[Nuclear Structure, pionic modes in medium Kisslinger catastrophe, pion group velocity]

PACS-Index 21.65.+f; 03.65.Ge; 24.10.Ht

NSF-ITP-81-70

Forward Angle Inelastic Scattering

G. F. Bertsch and O. Scholten

Institute for Theoretical Physics
University of California at Santa Barbara
Santa Barbara, California 93106

and

Cyclotron Laboratory
Michigan State University
East Lansing, Michigan 48824

(Recieved

ABSTRACT

The single-step contribution to nuclear inelastic scattering is analyzed in the independent particle model. We derive simple formulas for the single step total cross section and the response function, which are the two major ingredients in the theory. This description accounts for most of the cross section below an excitation energy of 40 MeV, seen in proton induced reactions at 200 and 800 MeV.

This work was supported in part by the National Science Foundation, Grant No. PHY77-27084.

SYSTEMATICS OF THE $\sigma\tau_-$ STRENGTH IN NUCLEI

G. Bertsch, D. Cha and H. Toki
National Superconducting Cyclotron Laboratory
and
Department of Physics
Michigan State University
East Lansing, Michigan 48824

[Nuclear Structure. Gamow-Teller states and L = 1 states in adjacent odd-odd mass nuclei of double closed shells. TDA and RPA calculation with zero range interaction.]

Abstract

The structure of the $\sigma\tau_-$ strength function is studied with a zero range interaction. The systematics of the giant Gamow-Teller state requires an interaction strength for $v_{\sigma\tau}$ of about 200 - 240 MeV-fm^3. While most of the strength goes to a state at high excitation, we find that ~20-30% of the strength remains at low excitation energy. The L = 1 states show considerable J-splitting, with a major peak at ≈20 MeV excitation. This peak contains components of J = 0, 1 and 2. Comparison with the experimental L = 1 energy shows that the momentum dependence of the $\sigma\tau$ interaction is small.

THE GIANT M1 STATES IN Zr ISOTOPES WITHIN THE SIMPLE SHELL MODEL

H. Toki, D. Cha and G. Bertsch
National Superconducting Cyclotron Laboratory
and
Department of Physics
Michigan State University
East Lansing, Michigan 48824

The newly observed M1 states in the (p,p') experiment on the Zr isotopes are considered within the simple shell model. The calculation with a constant strength δ-function interaction reproduces the excitation energies and the slight increase of the M1 strength at small momentum transfer with mass number. We need about a factor of 2 quenching to reproduce the cross sections at small angles, which is in accordance with the general finding for magnetic transitions.

[NUCLEAR STRUCTURE $^{90-96}$Zr; shell model calculations, 1^+ states]

Entropy production in high energy collisions

G. Bertsch

Physics Department, Michigan State University, East Lansing, Michigan 48824, and Institute for Theoretical Physics, University of California, Santa Barbara, California 93106

J. Cugnon

Institut de Physique, Université de Liège, Liège, Belgium

Abstract

The entropy production in high-energy collisions is computed in a Monte Carlo cascade model. For collisions of ^{40}Ca on ^{40}Ca at 800 MeV/n beam energy, the computed entropy is 4.4 per particle, about a unit higher than estimated from bulk dynamics. The particle correlation function of the final state is also computed, and is found to be in reasonable accord with a thermal distribution of the same entropy. With such low entropy values, most of the particles emerge in clusters, contrary to experiment. Thus the cascade calculation supports the conclusion of Siemens and Kapusta, that additional degrees of freedom become accessible in heavy ion collisions, beyond those in a conventional nuclear description.

NSF-ITP-81-34
SLAC PUB-2748 Misc.

Diffractive excitation in QCD

G. Bertsch*, S.J. Brodsky†, A.S. Goldhaber††,
and J.G. Gunion§

Institute for Theoretical Physics, University of California
Santa Barbara, California 93106

(Received)

ABSTRACT

Hadronic collision models based on Quantum ChromoDynamics predict remarkably large cross sections for diffractive scattering of hadrons on a nuclear target. The diffraction arises from the transparency of a nucleus to the portion of the projectile wavefunction having small transverse separation between its constituents. Correspondingly, the typical transverse momentum within the diffracted system is significantly enhanced. This QCD-based picture leads to large cross sections for diffractive charm production.

PACS numbers: 13.85.Hd, 24.90.+d

For submission to Can. J. Microbiol.

Denitrification and dissimilatory nitrate reduction to ammonium in digested sludge

HEINRICH F. KASPAR[1] and JAMES M. TIEDJE[2]

Departments of Crop and Soil Sciences and of Microbiology and Public Health, Michigan State University, East Lansing, Michigan, 48824

AND

RICHARD B. FIRESTONE[3]

Cyclotron Laboratory, Michigan State University, East Lansing, Michigan, 48824

[1]Current address: Cawthron Institute, P.O. Box 175, Nelson, New Zealand.

[2]To whom reprints should be addressed: J. M. Tiedje, Department of Crop and Soil Sciences, Michigan State University, East Lansing, MI 48824.

[3]Current address: Lawrence Berkeley Laboratory, University of California, Berkeley, CA.

A Kinetic Explanation for Accumulation of Nitrite, Nitric Oxide, and Nitrous Oxide during Bacterial Denitrification

Michael R. Betlach[1+] and James M. Tiedje[1, 2*]

Departments of Microbiology and Public Health[1]
and of Crop and Soil Sciences[2]
Michigan State University
East Lansing, Michigan 48824

Running head: Kinetics of bacterial denitrification

[+]Present address: Extraterrestrial Research Division
NASA Ames Research Center
Moffett Field, CA 94035

+

Journal article No. 9274 of the Michigan Agricultural Experiment Station.

TRANSPORT DE FAISCEAU POUR SPECTROSCOPIE IONS LOURDS A HAUTE RESOLUTION.

P. ROUSSEL et E. KASHY*
Institut de Physique Nucléaire
B.P. n° 1 - 91406 ORSAY Cédex France

Beam-transport system for high-resolution heavy-ion spectroscopy :

A method is given to adjust a beam-transport system to the requirements of high energy-resolution heavy-ion spectroscopy. The results of a test experiment performed on a MP tandem with a ^{12}C beam are shown. A drastic improvement in energy resolution is obtained for a kinematical factor $K = \frac{1}{p} dp/d\theta \sim 0.12$.

---

* adresse permanente : Michigan State University, East Lansing U.S.A.
(soutenu en partie par NSF-PHY-7822696)